FRACTAL NANOPARTICLES OF PHASE-SEPARATING SOLID SOLUTIONS: MORPHOLOGY-DEPENDENT PHASE EQUILIBRIA IN TUNGSTEN HEAVY PSEUDO-ALLOYS

Shishulin A.V.[1,2*], Potapov A.A.[3,4], Shishulina A.V.[5]

[1] Pleiades Publ., Ltd., Moscow, Russia,
[2] G.A. Razuvaev Institute of Organometallic Chemistry, Russian Academy of sciences, Nizhny Novgorod, Russian Federation, chichouline_alex@live.ru
[3] V.A. Kotel'nikov institute of radio engineering and electronics, Russian Academy of sciences, Moscow, Russian Federation
[4] JNU-IREE RAS Joint Laboratory of Information Technology and Fractal Processing of Signals, Jinan University, Guangzhou, China
[5] R.E. Alekseev Nizhny Novgorod State Technical University, Nizhny Novgorod, Russian Federation

In this paper, we simulate thermodynamically the morphology-dependent phase equilibria in core-shell nanoparticles of a phase-separating solid solution using the example of W-Cr heavy alloy. The morphology of a nanoparticle is described in the framework of the fractal geometry methods. It is shown that there are two possible heterogeneous states in a nanoparticle while the compositions of phases in both states differ from each other. The dependences of mutual solubilities of components on the temperature are obtained while the behavior of these dependences significantly differs depending on the particular state and the morphology of nanoparticle under consideration. In nanoparticles of a very complicated morphology, the phase separation itself gets suppressed and the nanoparticle remains in the homogeneous state at the temperatures significantly below the macroscopic value of the upper critical dissolution temperature. The demonstrated regularities are explained based on three mechanisms of reducing the free energy of the system and the "competition" between them. In the final section, a method for calculating the equilibrium size distributions and average characteristics of nanoparticle ensembles is described along with a technique of measuring nanoparticle fractal dimensions based on the microscopy data.

Keywords: nanoparticles, phase separation, tungsten, chromium, fractal dimension.

1. Introduction

In recent years, one of the main development vectors of the contemporary metallophysics is represented by investigating the unique set of properties of nanoparticle-fabricated samples which are resulted from the formation an ultrafine-grained structure in such materials. The structure of this type is generally obtained using the up-to-date additive powder metallurgy technologies [1-5] including the selective laser melting (SLM), selective laser sintering (SLS) and, especially, spark plasma sintering (SPS) methods [1, 2]. The last technique consists in the high-rate heating of nanopowders in a special conducting (graphite) mold due to the propagation of short (dozens of milliseconds) high-power current pulses through it. The sintering is carried out in the vacuum or in the atmosphere of an inert gas, the one-axis pressure being applied to the sample at the same time. An ultrafine-grained structure is obtained and the grain growth process is hampered in the case of the considered technologies as a result due to the possibility of dramatically high heating rates (up to 2000 – 2500 °C/min). It also necessary to mention that the SPS technology provides a number of "knobs" which make it possible to influence on the key characteristics of the obtained nanostructure of a metal sample through tuning the value of the applied pressure, heating temperature and heating time, heating and cooling rates etc. even in the course of the sintering process.

One of the primary objects of applying the developed additive manufacturing methods are the nanostructured tungsten-based heavy pseudo-alloys (the components of those are boundedly soluble in each other while the material is obtained using the different methods from the direct alloying) including the W_{1-x}–Cr_x ones [1-4, 6, 7]. Along with the significant fracture resistance under the dynamic loading conditions [6], the alloys of this system are characterized, for example, by the possibility of self-passivation [1] and a

dramatically high corrosion resistance at high temperatures [1, 2]. These ones and many other features [4] together provide a large number of biomedical, construction and special applications for such alloys.

At the mascoscopic scale, the W_{1-x}–Cr_x to not form a continuous series of solid solutions and undergo the phase separation with the upper critical dissolution temperature (UCDT) at 1906 K without any intermetallic phases [1, 7-9]. In the case of the additive powder metallurgy technologies being applied, the primary ways of controlling the physico-chemical properties of such materials consist in the formation of super-saturated solid solutions [1, 4] as well as of grain-boundary segregations with excessive contents of the dissolved component [7]. At the same time, in the analysis of phase equilibria in systems of a small volume, it is necessary to take into account several characteristic features. These peculiarities manifest themselves in significant dependences of mutual solubilities of components and equilibrium volume fractions of co-existing phases on the volume [9-20], shape of a nanoparticle [12-14, 18], thermodynamical characteristics of the surrounding environment [20] and several other factors [15, 17, 19]. The equilibrium phase compositions of small-volume systems are significantly different from the phase compositions of the same systems in the bulk state and can be modeled using the methods of equilibrium chemical thermodynamics [21] and several other approaches [22] (the applicability of thermodynamical methods in the analysis of phase equlibria in small-volume systems as well as their applicability limits are discussed in [23]). The experimental observations of the abovementioned effects are described, for example, in [24, 25].

2. Mathematical model of the phase separation in nanoscale particles

In the bulk state, the phase equilibria in the W_{1-x}-Cr_x system are represented by the classical Becker curve [1, 8, 9]: the components are boundedly soluble in each other below the temperature of ~1906 K. As the system to be modeled below, we consider equiatomic nanoparticles of various shapes; below the UCDT, the nanoparticle contains a spherical-shaped inclusion (which is hereinafter referred as "*core*-phase") of a solid-solution surrounded by a solid-solution layer ("*shell*-phase") of a given shape. The nanoparticle volume is characterized by the effective diameter (d_{eff}, the diameter of the sphere, the volume of which being equal to the one of the considered nanoparticle). In a closed binary system with the *core-shell* configuration, the conservation conditions of matter interrelate the nanoparticle effective diameter, total amount of matter in the system (n), numbers of moles of each component (n_i, indices i= 1, 2 correspond to chromium and tungsten, respectively) and concentrations of components i in phases j (x_{ij}, indices j = c, s correspond to *core*- and *shell*-phases, respectively) [18]:

$$\pi d_{\text{eff}}^3 \big/ 6 = \sum_j V_j,\ n_1 = xn,\ n_2 + n_1 = n,\ n_i = \sum_j n_{ij},\ V_j = \sum_i n_{ij} V_i,\ x_{ij} = n_{ij} \big/ \sum_i n_{ij}. \tag{1}$$

Here, V_j and V_i are the volume of phase j and the molar volume of component i, respectively. The molar volumes are $V_1 = 7.23$ cm³/mol, $V_2 = 9.53$ cm³/mol. x=0.5 in the case of equiatomic particles [9, 15].

In order to provide a general description of all the possible nanoparticle geometric configurations including the most complicated and irregular ones, the fractal geometry approach is used [18, 26-28]. In the framework of this approach, the nanoparticle shape is characterized by its fractal dimension D which relates its surface area A_s to its volume (effective diameter d_{eff}): $A_s = C\left(\pi d_{\text{eff}}^3 \big/ 6\right)^{2/D}$. Without any losses of generality, constant C is assumed to be $C = 4\pi$ [18, 26-28]. For regular simple structures, $D \equiv 3.00$, in their turn, the structures of a complicated and irregular morphology correspond to the values of $D < 3.00$ while D is also non-integer.

The examples of structures with various D are given in Refs. [27, 28]. Fractal dimension D of a nanoparticle can also be expressed in terms of the nanoparticle surface-to-volume ratio (k): $k(V,D) = V^{2/D} \big/ \left(3V/4\pi\right)^{2/3}$, $V = \pi d_{\text{eff}}^3 \big/ 6$. The nanoparticles of 40 nm in effective diameter and fractal dimensions of 2.60, 2.75 and 2.90 correspond to the surface-to-volume ratio values of 2.51, 1.72 and 1.23, respectively.

In the considered system, the characteristics of the equilibrium state are obtained by minimizing the Gibbs function (g) per one mole of matter including the energy contributions of all interface boundaries:

$$g = \sum_j \left(n_{1j} + n_{2j}\right) G_j\left(x_{1j},T\right) + \sigma_s A_s + \sigma_{cs} A_s,$$

$$G_j\left(x_{1j},T\right) = A_{\text{I}} x_{1j}\left(1 - x_{1j}\right) + A_{\text{II}} x_{1j}^2\left(1 - x_{1j}\right) + A_{\text{III}} x_{1j}\left(1 - x_{1j}\right)^2 + RT\left(x_{1j}\ln x_{1j} + \left(1 - x_{1j}\right)\ln\left(1 - x_{1j}\right)\right). \tag{2}$$

Here, σ_{cs} and σ_s are the surface energies of the inner (*core-shell*) and outer (*shell-*) interface boundaries while R is the universal gas constant. The parameters A_I, A_{II}, A_{III} are as follows: $A_I = 30202.0$; $A_{II} = 2635.5$; $A_{III} = 0$ [9, 15]. The energies of interface boundaries are calculated using the first approximation (this approach and the obtained results are not accompanied by any losses of generality, see also [17, 19]): $\sigma_{cs} = 0.5 \sum_j \sigma\left(x_{1j}\right)$, $\sigma\left(x_{1j}\right) = \sigma_1 x_{1j} + \sigma_2 \left(1 - x_{1j}\right)$, $\sigma_s = \sigma_1 x_{1s} + \sigma_2 \left(1 - x_{1s}\right)$. Here, $\sigma_1 = 0.657$ J/m^2, $\sigma_2 = 1.110$ J/m^2 [9, 15].

In the case of the properties of small-volume systems being considered in the framework of the thermodynamical approach, the problem of the thermodynamics applicability at the nanoscale and its lower boundary cannot be ignored. As the authors of [23] have noted, it is the most appropriate to apply the theoretical approaches based on the fluctuation theory to determine the applicability limits of chemical thermodynamics. Indeed, spontaneous fluctuations of thermodynamical characteristics (associated with the discreteness of the atomic-molecular structure of any system, being increased with a decrease in the amount of the matter which forms the system) represent the natural limitations on the application of thermodynamical approaches: if the fluctuation values of a parameter get comparable with the values of the parameter, this fact testifies, on the one hand, to the inadequate application of the thermodynamics techniques in this case, on the other hand, to the instability of the considered system itself as well as to the tendency of its decomposition due to fluctuations.

In [23], the authors have analyzed the fluctuations of temperature and surface tension of nanostructures. The temperature is taken into account by the authors (instead of the density, for example) due to the fact that the temperature plays the role of the "only state parameter introduced in the thermodynamics in addition to the mechanical variables such as pressure P and volume V" for simple systems. Meanwhile, the structure stability of small-volume systems directly depends on the value of a temperature fluctuation. In order to estimate the absolute value of the root-mean-square temperature fluctuation δT, the following expression can be used: $\delta T = T\sqrt{R/C_X N}$. Here, X is the variable (or the set of variables) which remain constant in the considered case; N is the number of molecules and atoms which are contained in the considered systems; R is the universal gas constant; C_X is the molar heat capacity at $X = $ const. In [23], it is assumed that $X = P$ while the isobaric molar heat capacity is included into the abovementioned expression (in the considered case, the surface contribution to the heat capacity of a nanosystem is not taken into account since the value of the temperature derivative of the surface enthalpy (introduced for the first time by E. Guggenheim) does not exceed a fraction of a cent of heat capacity C_P according to the authors' early assessments). The results of calculating δT are given in Table 1 of [23] where nanoscale droplets of *n*-butane and solid nanoscale aluminum and sodium particles have been used as model systems. The calculations show that the value of δT does not exceed a few percent in all the three cases even for a system containing $N = 100$ atoms or molecules (δT decreases with an increase in N).

In their turn, the following expression is used in order to calculate the relative fluctuations $\Delta\sigma/\sigma$ of the surface tension:

$$\frac{\Delta\sigma}{\sigma} = \begin{cases} \sqrt{\dfrac{kT\beta_T}{12\pi r^3}}, & r \leq r_{ch} \\ 0, & r > r_{ch} \end{cases}$$

where k is the Boltzmann constant; r is the radius of a nanoparticle; β_T is the isothermal compressibility; r_{ch} is the characteristic size determined as follows: in the case $r > r_{ch}$, the surface tension of a nanoparticle can be considered to be equal to its macroscopic value; in the case $r \leq r_{ch}$, it is assumed that the dependence of the surface tension on the system size is described by the linear formula of A.I. Rusanov: $\sigma = Kr$ where K is the proportionality factor which is commonly estimated based on numerical simulations or empirically.

As it is demonstrated in Table 2 of [23], where the estimates of fluctuations for several pure metals are given, the fluctuation values are no more than a fraction of a cent even for a cluster containing 12 atoms. The considered estimates can also be accompanied by the considerations of M.N. Magomedov on the minimum nanoparticle size at which the differences between solid and liquid phases disappear. The geometric

characteristics of the objects studied in this paper correspond to the area where the applicability of the thermodynamical approach leaves no doubt.

3. Simulation results and discussion

The Gibbs function of a two-components phase-separating system with a *core-shell* structure (1-2) has two minima which correspond to two-phase states with different mutual positions of co-existing phases. Below, the state where the *core*-phase is formed with tungsten (while the *shell*-phase is chromium based) is referred as "state 1". Vice versa, chromium prevails in the *shell*-phase in state 2. In the case the bulk nanoparticles are dealt with, the minima of the Gibbs function corresponding to each state are symmetric and characterized by equal energies while the compositions of co-existing *core*- and *shell*-phases do not depend on the state, which emerges in the nanoparticle. The compositions of *core*-and *shell*-phases in the bulk structures are also independent on particle size and morphologyand match the reference data [8]. At the nanoscale, due to the significant increase in the energy contribution of all the interface boundaries in the system, the minima of the Gibbs function shift in comparison with the ones of bulk structures. As a result, the compositions of *core*- and *shell*-phases depend on the mutual arrangement of co-existing phases, being different in states 1 and 2, as well as on the size and morphology of the considered nanoparticles. The free energy of nanoparticles in state 1 is lower than the one of state 2, i.e., state 2 becomes metastable.

The effects demonstrated below result from the tendency of the nanosystem to reduce its free energy: in a *core-shell* structure; such reduction can be realized according to the three mechanisms. The terms introduced in [17] being used, these mechanisms are as follows:

- *volume-controlled segregation*: transferring the matter form the inner phase (*core-*) into the outer one (*shell-*) leading to a decrease in the area of the internal (*core-shell*) interface boundary (this mechanism is hereinafter denoted as "mechanism 1");

- *surface energy-controlled segregation*: enriching predominantly the outer (*shell-*) phase with the component with the lower surface energy leading to a decrease in the energy of the external interface boundary (the energy contribution of the internal one being much lower practically always; this mechanism is hereinafter denoted as "mechanism 2");

- *suppression*: maintaining the homogeneous state of the system, the phase-separation process being suppressed. Physically, this mechanism stems from reducing the upper critical dissolution temperature down to the value below the considered one (this mechanism is hereinafter denoted as "mechanism 3"). In the case mechanism 3 being realized, the minimum of the Gibbs function corresponding to the considered heterogeneous state disappears, being replaced by the one corresponding to the homogeneous configuration.

In the considered system, tungsten is characterized by higher values (in comparison with chromium) by higher values of the molar volume and surface energy at the same time. The effective diameter of the nanoparticles simulated below is 40 nm. The nanoparticle composition is equiatomic.

For both states, Fig. 1 illustrates the dependence of the solubility limits of chromium in tungsten on the nanoparticle morphology and temperature. The realization of the considered effects is the most vivid for state 2: the lower the volume of a nanoparticle is and the more complicated the morphology of a nanoparticle is (the lower the fractal dimension is), the higher the solubility of chromium in tungsten. For example, being equal to ~9 at. % (the values for bulk structures are given in Fig. 1 with the solid line without markers) for macroscale particles at $T = 1300$ K, the solubility limit demonstrates a dramatic increase up to ~14 (for $D = 2.90$) and ~15 at. % ($D = 2.80$). At the same time, variations of the fractal dimension of a nanoparticle in state 2 lead to small changes in the solubility of W in Cr. For state 1, the solubility of chromium in tungsten shows a lower sensitiveness to the changes in D (which is accompanied, however, by a significant reduction of the mentioned solubility limit with a decrease in the nanoparticle effective diameter).

Fig. 2, in its turn, demonstrates how the nanoparticle morphology influences on the solubility of W in Cr in state 1. Firstly, the lower the fractal dimension is, the lower the solubility limit of tungsten in chromium turns out to be. Secondly, the relation between the nanoscale solubility limit and the bulk one depends on the fractal dimension of a nanoparticle. In detail, the solubility of tungsten in chromium in nanoparticles is lower than the one in the bulk state in the case of $D < 2.90$. In the case of "regular" nanoparticles ($D = 3.00$), meanwhile, the solubility limit exceeds the bulk value at "high" temperatures near the UCDT.

At lower temperatures, however, the solubility limit is somewhat lower in comparison with the one for macro-sized particles. Taking into account the mechanisms listed above, the demonstrated regularities can be

explained as follows: "complicating" the morphology and decreasing the effective diameter of a nanoparticle in state 2 leads to the predominant implementation of mechanism 2 ("*surface energy-controlled segregation*"); the atomic fraction of Cr in the *shell*-phase grows up.
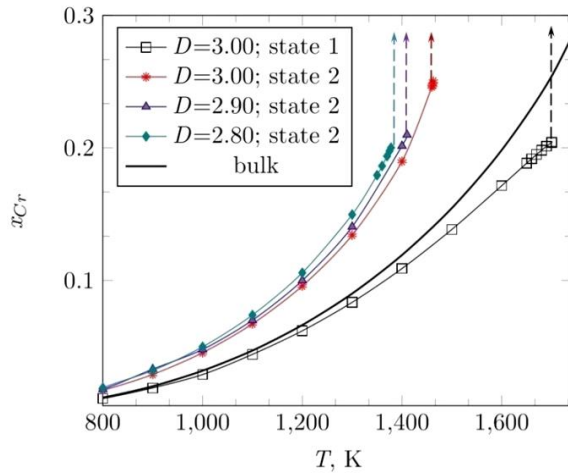

Fig. 1. Temperature - dependent phase equilibria (the chromium solubility in tungsten, atomic fractions) for nanoparticles in different states of the *core-shell* structure for various values of *D*.
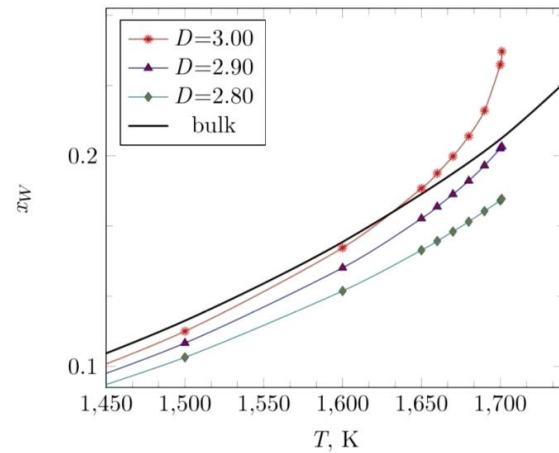
Fig. 2. Temperature-dependent phase equilibria (the tungsten solubility in chromium, atomic fractions) for nanoparticles in state 1 for various values of *D*.

The same mechanism 2 is characteristic for "regular" ($D = 3.00$) nanoparticles in state 1 at "low" temperatures (a decrease in the atomic fraction of W in the *shell*-phase is observed). At "higher" temperatures, at the same time, mechanism 1 ("*volume-controlled segregation*") is realized while the tungsten content is increased in the *shell*-phase. If the nanoparticle morphology becomes more complicated (i.e., the fractal dimension of a nanoparticle is reduced) at any temperature in state 1, the realization of mechanism 2 manifests itself (in more detail, the "competition" between the mechanisms of reducing the free energy is discussed in [16, 17, 19]).In the Fig. 1, the vertical dashed lines represent the temperatures at which mechanism 3 ("*suppression*") is implemented in nanoparticles. At these temperatures, the minimum of the Gibbs function (which corresponds to the heterogeneous state 2) disappear with the appearance of another one in the position of the homogeneous state without the phase separation.

The "*suppression*" temperature for state 1 is higher than the one for state 2 (as demonstrated in Fig. 1): between these temperatures for states 1 and 2, the heterogeneous state 1 and the homogeneous state formed instead of the heterogeneous state 2 are the possible ones in the system. Above the "*suppression*" temperature for state 1, the homogeneous configuration becomes the only possible one. As mentioned above, the "*suppression*" temperatures for nanoparticles can be associated with the nanoscale UCDT values for states 1 and 2; in both cases the UCDTs are much lower in comparison with the bulk values, especially for nanoparticles in state 2: the UCDT reduction with a decrease in the fractal dimension reaches the values of hundreds degrees. The demonstrated results can be accompanied by several other non-trivial effects in small-volume structures, e.g., by the effect of the chemical composition. In bulk structures, a variation of the initial composition of the considered system leads only to changes in the volume fractions of co-existing phases (directly according to the so-called "lever rule") but has no influence on the equilibrium phase composition. In small-volume systems, in their turn, not only the volume fractions but also the compositions of *core-* and *shell*-phases (and co-existing phases in the most general case) at equilibrium depend on the initial composition. This effect is generic for nanoscale structures, being explained by the realization of different mechanisms of lowering the free energy of the system in the case of nanoparticles of different compositions (see [17, 19] for more details).

In real-life fabrication processes, the nanoparticle ensembles are dealt with instead of individual nanoparticles, being characterized by the size and shape distributions. As shown by us in [26, 28], the equilibrium size distributions for a free-dispersed system formed by nanoparticles with fractal dimension *D* can be expressed as follows:

$$f_D\left(\phi_p, D, N\right) \sim \exp\left(-\frac{\gamma A_{sp}(D) + RT \ln f_p}{RT}\right), \quad f_p = \frac{N}{N - \phi_p} \exp\left\{\pi\left(\sqrt{\frac{2}{3}}\left(N - \phi_p\right) - \sqrt{\frac{2}{3}N}\right)\right\}.$$

Here, $\phi_p = \omega\left(d_{eff}/d_{at}\right)^3$ is the so-called "stoichiometric number" of a nanoparticle (the number of atoms in a nanoparticle), $A_{sp}(D)$ is the specific surface area of the nanoparticle ensemble, γ is the surface energy of the material in the considered external environment (see also some remarks in Ref. [20]); ω is the lattice packing density, N is the total number of atoms in the system, d_{at} is the atomic diameter.

The suggested calculation technique provides the results which are in perfect accordance with the experimentally observed distributions (see [26] and Refs. therein). the estimates can be obtained which make it possible to model the thermodynamical conditions for the realization of optimal average geometric characteristics of nanoparticles leading to the optimal phase composition as well to predict the degree at which the equilibrium phase compositions and the set of composition-dependent functional properties are "blurred" in an ensemble. For example, average fractal dimension $\langle D \rangle$, average stoichiometric number $\langle \phi_p \rangle$ and average effective diameter d_{eff} of nanoparticles in the ensemble can be calculated as follows [28]:

$$\langle D \rangle = \frac{\sum_i D_i \int f_D\left(D_i, \phi_p, N\right) d\phi_p}{\Omega(N)}, \quad \langle \phi_p \rangle = \frac{\sum_i \int \phi_p f_D\left(D_i, \phi_p, N\right) d\phi_p}{\Omega(N)},$$

$$\langle d_{eff} \rangle = \Omega(N)^{-1} d_{at} \sum_i \int f_D\left(D_i, \phi_p\right) d\phi_p, \quad \Omega(N) = \sum_i \int f_D\left(D_i, \phi_p, N\right) d\phi_p.$$

Here, the limits of the integration over ϕ_p belong to range $[1, N]$ while the sample of distributions is considered where $D_i \in (2, 3)$ with an arbitrarily selected step [26, 28].

The fractal dimension of nanoparticles can be estimated based on the optical or electron microscopy data using various methods including the so-called "box-counting technique" [29]. In the framework of the mentioned approach, the image of the considered nanoparticle ensemble is converted into a monochrome one which is then divided into square equal-area cells. In order to calculate the fractal dimension, the image divided into cells is transformed into a square matrix. If the brightness of a cell exceeds the preliminarily selected brightness threshold value (B_{th}), such a cell corresponds to the matrix cell with the value of 1. Otherwise, an image cell is represented by a matrix cell with the value of 0. Based on this transformation, fractal dimension D is calculated using the following expression: $S = AL^D$ where S is the number of matrix cells with the value of 1; L is the matrix rank; A is the factor which matches dimensions. The dependence is obtained using the least squares method: the matrix rank being sequentially decreased (the cell size being increased) by 2, 4, 8, … times provided that the value of 1 is assigned to the cells which contain at least one pixel of the initial image, the brightness of which exceeds the selected threshold value.

In the general case, the calculated fractal dimension is sensitive to the value of B_{th}, being varied in a wide range when changing B_{th}. For selecting the correct value of B_{th}, the "calibration" dependence ($D(B_{th})$) is constructed. The sensitivity of the fractal dimension to the brightness threshold is represented by the inclination angle of curve $D(B_{th})$. An example of such "calibration" dependences is demonstrated in [30].

In the formal consideration, the random uniformly distributed white noise is characterized by its fractal dimension as well as by the relation between D and the brightness threshold in the form of a smooth monotonously decreasing function as follows:

$$D(B_{th}) = 2 + \frac{\ln\left(1 - \frac{B_{th}}{B_{th}^{max}}\right) - \ln A}{\ln L}, \quad S = L^2\left(\frac{B_{th}^{max} - B_{th}}{B_{th}^{max}}\right) = AL^D.$$

In the case of a square image, $A = 1$. However, the dependence of D on matrix rank L does not allow considering the random noise as an appropriate fractal object for the application of the box-counting techniques. The monochrome images of the classical fractal objects (Koch snowflakes, Sierpinski carpets, fractal trees etc) are characterized by $D = \mathrm{const}$, $A = \mathrm{const}$ for any B_{th}. For real images which represent

superpositions of fractal structure and noise, dependence $D(B_{th})$ contains straight sections, steps as well as extrema and inflection points. The correct brightness threshold value corresponds to the straight section within which the deviation of dependence $\ln S = D \ln L + \ln A$ from a straight line is minimal. This section is found based on the minimum value of the first derivation of dependence $D(B_{th})$. The absence of a well-pronounced straight section can result from the heterogeneity of optical properties of nanoparticles or to the insufficient image quality.

4. Conclusion

The performed thermodynamical analysis of how the phase equilibria in nanoscale particles of phase-separating solid solutions depend on the particle morphology using the example of W-Cr heavy pseudo alloy leads to the following conclusions.

1. A nanoparticle with a *core-shell* structure has two possible two-phase states which correspond to different mutual arrangements of co-existing tungsten-based and chromium-based phases. Unlike systems in the bulk state where both phases have equal free energies and compositions of *core-* and *shell*-phases, in nanoscale particles, the phase compositions are considerably different in each state.

2. The temperature range in which the heterogeneous state is stable significantly shrinks with reducing the volume of a nanoparticle and "complicating" its morphology. The upper critical dissolution temperatures for each state of the *core-shell* structure are also different, being both reduced with a decrease in the particle size and fractal dimension.

3. The equilibrium phase composition of nanoparticles in each state depends on the particle morphology while the pattern itself of the dependences of mutual solubilities significantly differs for particles of various shapes in different states. This fact is associated with the occurrence of three different mechanisms ("volume-controlled segregation", "surface energy-controlled segregation" and "suppression") which can manifest themselves at the same time and even be "competing".

The obtained reguliarities also demonstrate an additional "knob" which makes it possible to tune multiple composition-dependent functional properties of nanostructured materials (including electrical and thermal conductivity, resistivity to corrosion, elastic properties etc) through the taking into account the specific influence of morphology factors on the phase composition at the nanoscale. Such considerations could also be accompanied either with the up-to-date techniques of the controllable synthesis of nanoparticles with a given shape or with the methods of describing and predicting various properties of nanoparticle ensembles. In the latter case, our considerations can be helpful in predicting the range possible variations of nanoparticle phase compositions as well as the degree at which the corresponding functional properties are "blurred" in an ensemble.

REFERENCES

1   Vilémová M., Illková K., Lukáš F., et al. Microstructure and phase stability of W-Cr alloy prepared by spark plasma sintering. *Fus. eng. des.*, 2018, Vol. 127, pp. 173 – 178. doi:10.1016/ j.fusengdes.2018.01.012.

2   Hou Q.-Q., Huang K., Luo L.-M., Tan X.-Y., et al. Microstructure and its high temperature oxidation behavior in W-Cr alloys prepared by spark plasma sintering. *Materialia,* 2019, Vol. 6, p.100332. doi:10.1016/j.mtla.2019.100332.

3   Bose A., Schuh C.A., Tobia J.C., et al. Traditional and additive manufacturing of a new tungsten heavy alloy alternative. *Int. j. refract. met. hard mater.,* 2018. Vol. 73, pp. 22 – 28. doi:10.1016/j.ijrmhm.2018.01.019.

4   Tilmann W., Fehr A., Heringhaus M. Mechanical milling to foster the solid solution formation and densification in Cr-W-Si for hot-pressing of PVD target materials. *Adv. powder technol.*, 2021, Vol.32, No.6, pp. 1927 – 1934. doi:10.1016/j.apt.2021.04.001.

5   Olakanmi E.O., Cochrane R.F., Dalgarno K.W. A review of selective laser sintering/melting (SLS/SLM) of aluminium alloy powders: Processing, microstructure, and properties. *Prog. mater. sci.*, 2015. Vol. 74, pp. 401 – 477. doi:10.1016/j.pmatsci.2015.03.002.

6   Cordero Z.C., Carpenter R.R., Schuh C.A., et al. Sub-scale ballistic testing of an ultrafine grained tungsten alloy into concrete targets. *Int. j. impact eng.*, 2016, Vol. 91, pp. 1 – 5. doi:10.1016/j.ijimpeng.2015.11.013.

.

7   Chookajorn T., Park M., Schuh C.A. Duplex nanocrystalline alloys: entropic nanostructure stabilization and a case study on W-Cr. *J. mater. res.*, 2015., Vol. 30, No. 2, pp. 151 – 162. doi:10.1557/jmr.2014.385.

8   Udovskii A.L., Karpushkin V.N., Nikishina E.A. A method for autonomous thermodynamic assessment of phase diagrams of binary systems containing p disordered phases of variable composition and q phases of constant composition at $(p, q) \leq 10$. *Metally,* 1991. No. 4, pp. 87 – 103 [in Russian].

9   Shishulin A.V., Shishulina A.V. Equilibrium phase composition and mutual solubilities in fractal nanoparticles of the W-Cr heavy pseudo-alloys. *Physical and chemical aspects of the study of clusters, nanostructures and nanomaterials,* 2019, No. 11. pp. 380 – 388. doi:10.26456/pcascnn/2019.11.380.

10 Bajaj S., Haverty M.G., Arróyave R., Goddard W.A., Shankar S. Phase stability in nanoscale material systems: extensions from bulk phase diagrams. *Nanoscale*, 2015, Vol. 7, No. 9868. doi:10.1039/C5NR01535A.

11 Shirinyan A., Wilde G., Bilogorodskyy Y. Melting loops in the phase diagram of individual nanoscale alloy particles: completely miscible Cu-Ni alloys as a model system. *J. mater. sci.*, 2020. Vol. 55, pp. 12385 – 12402. doi:10.1007/s10853-020-04812-2.

12 Mendoza-Pérez R., Muhl S. Phase diagrams of refractory bimetallic nanoalloys. *J. nanopart. res.*, 2020, Vol. 22, No. 36. doi:10.1007/s11051-020-05035-x.

13 Geoffrion L.-D., Guisbiers G. Chemical ordering in Bi_{1-x} –Sb_x nanostructures: Alloy, janus or core-shell? *J. phys. chem., C.* 2020, Vol.124, No.25, pp. 14061 – 14068. doi:10.1021/acs.jpcc.0c04356.

14 Geoffrion L.D., Guisbiers G. Physico-chemical properties of selenium–tellurium alloys across the scales. *Nanoscale Adv.*, 2021. Vol.3, No.14, pp. 4254 – 4270. doi:10.1039/D1NA00087J.

15 Shishulin A.V., Fedoseev V.B. Effect of initial composition on the liquid–solid phase transition in Cr-W alloy nanoparticles. *Inorg. mater.,* 2019. Vol.55, No.1, pp. 14 – 18. doi:10.1134/S0002337X19010135.

16 Ghasemi M., Zanolli Z., Stankovski M., Johansson J. Size- and shape-dependent phase diagram of In-Sb nanoalloys. *Nanoscale*, 2015, Vol. 7, pp. 17387 – 17396. doi:10.1007/s10891-020-02182-9.

17 Shishulin A.V., Potapov A.A., Shishulina A.V. The initial composition as an additional parameter determining the melting behavior of nanoparticles (a case study on Si_x-Ge_{1-x} alloys). *Eurasian phys. tech. j.,* 2021, Vol. 18, No.4, pp. 5 – 13. doi:10.31489/2021NO4/5-14.

18 Guisbiers G., Khanal S., Ruiz-Zapeda F., Roque de la Puente J., Yakaman M.-J. Cu-Ni nanoalloy: mixed, *core-shell* or janus nanoparticles? *Nanoscale*, 2014, Vol. 6, pp. 14630-14635. doi:10.1039/C4NR05739B.

19 Shishulin A.V., Shishulina A.V. One more parameter determining the stratification of solutions in small-volume droplets. *J. eng. phys. Thermophys,* 2022, Vol. 95, No. 6, pp. 1374 – 1382. doi:10.1007/s10891-022-02606-8.

20 Shishulin A.V., Fedoseev V.B., Shishulina A.V. Environment-dependent phase equilibria in a small-volume system in the case of the decomposition of Bi-Sb solid solutions. *Butlerov commun.*, 2017. Vol. 51, No. 7, pp. 31 – 37 [in Russian].

21 Guisbiers G. Advances in thermodynamic modeling of nanoparticles. *Adv. phys. X.*, 2019, Vol. 4, No.1, 1668299. doi:10.1080/23746149.2019.1668299

22 Magomedov M.N. On the statistical thermodynamics of a free-standing nanocrystal: silicon. *Cryst. rep.*, 2017, Vol. 63, No. 3, 480 – 496. doi:10.1134/S1063774517030142.

23 Samsonov V.M., Demenkov D.E., Karcharov V.I., Bembel A.G. Fluctuation approach to the problem of thermodynamics applicability to nanoparticles. *Bull. Russ. acad. sci.: phys.*, 2011. Vol. 75, No. 8, pp. 1073 – 1077. doi:10.3103/S106287381108034X.

24 Straumal B.B., Mazilkin A.A., Straumal P.B., Gusak A.M., Baretzky B. Shift of lines in phase diagrams for nanograined materials. *Adv. struct. mater.*, 2013. Vol. 4, pp. 265 – 285. doi:10.1007/8611_2010_29.

25 Radnóczi G., Bokányi E., Erdélyi Z., MisjákF. Size-dependent spinodal decomposition in Cu–Ag nanoparticles. *Acta mater.*, 2017.Vol. 123., pp. 82– 89. doi:10.1016/j.actamat.2016.10.036

26 Fedoseev V.B., Shishulin A.V. On the size distribution of dispersed fractal particles. *Tech. phys.*, 2021. Vol. 66, No. 1, pp. 34 – 40. doi:10.1134/S1063784221010072

27 Shishulin A.V., Potapov A.A., Shishulina A.V. On the transition between ferromagnetic and paramagnetic states in mesoporous materials with fractal morphology. *Eurasian phys. tech. j.,* 2021, Vol. 18, No.2, pp. 6 – 11. doi:10.31489/2021NO2/6-11.

28 Shishulin A.V., Potapov A.A., Shishulina A.V. Several notes on the lattice thermal conductivity of fractal-shaped nanoparticles. *Eurasian phys. tech. j.,* 2022, Vol. 19, No.3, pp. 10 – 17. doi:10.31489/2022NO3/10-17.

29 Li J., Du Q., Sun C. An improved box-counting method for image fractal dimension estimation. *Pattern recognit*, 2009. Vol. 42, pp. 2460 – 2469. doi:10.1016/j.patcog.2009.03.001.

30 Fedoseeva E.N., Fedoseev V.B. Interaction of chitosan with benzoic acid in solution and films. *Polymer sci. Ser. A.*, 2011. Vol. 53, No. 11, pp. 1040 – 1046. doi:10.1134/S0965545X1110004X.